

Preliminary data on subsolidus phase equilibria in the $\text{La}_2\text{O}_3\text{-Al}_2\text{O}_3\text{-Mn}_2\text{O}_3$ and $\text{La}_2\text{O}_3\text{-Al}_2\text{O}_3\text{-Fe}_2\text{O}_3$ systems

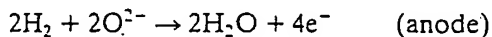
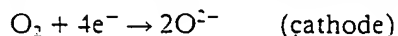
M. HROVAT, J. HOLC, D. KUŠČER, Z. SAMARDŽIJA, S. BERNIK
Jožef Stefan Institute, University of Ljubljana, Jamova 39, 61000 Ljubljana, Slovenia

BEST AVAILABLE COPY

A fuel cell is a device for direct conversion of chemical energy into electrical energy. Oxidant is fed to the cathode and reducing agent (fuel) to the anode. The electrolyte, through which the ion current flows, also prevents the mixing of oxidant and fuel. This concept is more than 150 years old. The principle of fuel cell operation was reported in 1839 by Sir William Grove [1]. His fuel cell used dilute acid as an electrolyte, and oxygen and hydrogen as oxidant and reducing agent, respectively.

High temperature solid oxide fuel cells (SOFC) work at temperatures up to 1000 °C. The solid electrolyte in SOFC cells is usually yttria-stabilized cubic zirconia (YSZ). The oxygen accepts electrons at the cathode and moves as an ion through the dense ZrO_2 ceramic. At the anode ions combine with fuel and release electrons. The fuel is usually either hydrogen, an H_2/CO mixture or hydrocarbon because the high temperature of operation makes possible the internal (*in situ*) reforming of hydrocarbons with water vapour [2].

The electrode reactions (for hydrogen as fuel) are:



The "force" driving the oxygen ions through the electrolyte is the concentration gradient of oxygen between the cathode and the anode side.

The advantage of SOFC is the high efficiency of 50–60% while some estimations are even up to a yield of 70–80% [3–6]. Also, nitrous oxides are not produced and the amount of CO_2 released per kilowatt is around 50% less than for power sources based on combustion. Annually, around 10⁹ US\$ is invested into research and development of fuel cells [7, 8].

Because of the high operating temperatures of SOFC the choice of materials is mainly limited to ceramics. As already mentioned, the solid electrolyte, which must have as high an ionic and as low an electronic conductivity as possible, is usually ZrO_2 stabilized with Y_2O_3 . The interconnect, which must withstand both oxidizing and reducing atmospheres, is based on doped LaCrO_3 . It must have high electronic and low ionic conductivity.

The electrodes (cathode and anode) must be porous to permit the diffusion of oxygen and fuel to the zirconia electrolyte, and must have high electrical conductivity. Metallic nickel is usually used as anode material. To prevent sintering of Ni particles

at fuel cell operating temperatures, Ni grains are incorporated in the zirconia matrix. Due to the high operating temperatures and oxidizing atmosphere on the cathode side, only noble metals, such as platinum, or oxides with low resistivity can be used for electrodes. Noble metals are less suitable, partly because of problems with long-term stability, but mostly because of their high cost. At present semiconducting oxides such as perovskites based on LaMnO_3 or LaCoO_3 , doped with SrO and CaO , are most often used as cathode materials. For an excellent and comprehensive review of materials for SOFC, see [9].

The open circuit voltage of an SOFC is expressed by the Nernst equation:

$$U_o = RT/4F \ln (PO_{2\text{oxy}}/PO_{2\text{red}})$$

where U_o is the open circuit voltage (Nernst potential), R is the gas constant, T is (absolute) temperature, F is the Faraday constant, $PO_{2\text{oxy}}$ is the partial oxygen pressure in the oxidant and $PO_{2\text{red}}$ is the partial oxygen pressure in the reducing agent. For the typical "working" conditions of the SOFC, i.e. a temperature of 1000 °C, air as an oxidant and a partial oxygen pressure in the wet hydrogen of 10^{-17} atm ($1 \text{ atm} = 1.013 \times 10^5 \text{ Pa}$; water vapour in the fuel at the anode side is the consequence of reactions with oxygen ions), the open circuit voltage is around 1 V. However, the operating voltage is lower, as seen from the following equation, and is typically around or less than 0.7 V:

$$U = U_o - IR - \eta_A - \eta_C$$

where U is voltage, U_o is the open circuit voltage (Nernst potential), IR is ohmic losses, η_A is polarization losses at the anode and η_C is polarization losses at the cathode. This is shown schematically in Fig. 1. The drawing is not to scale and the voltage and the current are given in arbitrary values. However, the

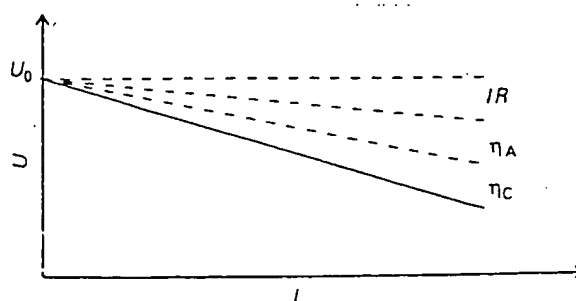


Figure 1. SOFC voltage profile against current density (schematic).

open circuit voltage is around 1 V and typical current densities are between 0.25 and 0.7 A cm⁻². The *IR* part, i.e. ohmic losses of the SOFC, is mostly due to the resistance of the solid electrolyte in the case of the planar type design, while in the case of tubular SOFC elements the resistance of the electrodes is also significant [10]. η_A and η_C are polarization losses related to irreversibilities in the electrode processes.

The electrode polarization losses are reduced if the electrode material possesses both high ionic and high electronic conductivity. This is illustrated schematically in Fig. 2 for the cathode. If the material is an electronic conductor only, the electrochemical reactions can occur solely at the three phase boundary (TPB) of the cathode, air (gas phase) and electrolyte (Fig. 2a). The thickness of the TPB is estimated to be around or under 1 μ m [11]. If the cathode material possesses mixed type conductivity, the reduction of oxygen can occur on the entire surface of the electrode (Fig. 2b). Therefore, many alternative cathode materials with mixed conductivity are being investigated for possible use in SOFCs. Two such interesting materials are doped LaFeO₃ and LaAlO₃. Doped LaFeO₃ possesses high mixed conductivity [12] and is therefore a good candidate for the SOFC cathode. Undoped LaAlO₃ is a dielectric, while doped LaAlO₃ becomes a mixed conductor [13].

As part of a study of undoped and SrO doped La(Mn, Al)O₃ and La(Fe, Al)O₃ as possible SOFC cathodes, subsolidus phase equilibria in the La₂O₃-rich part of the La₂O₃-Al₂O₃-Mn₂O₃ and La₂O₃-Al₂O₃-Fe₂O₃ systems were investigated. In this letter the preliminary data on solid solubility between LaMnO₃-LaAlO₃ and LaFeO₃-LaAlO₃, obtained by energy-dispersive spectroscopy (EDS)

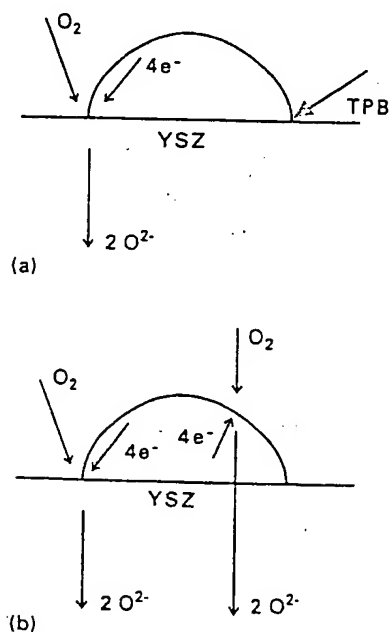


Figure 2 Schematic of the electrochemical reactions on the SOFC cathode. (a) If the material is an electronic conductor, the reactions can occur only at the TPB. (b) If the cathode material possesses mixed type conductivity the reduction of oxygen can occur over the entire surface of the electrode.

microanalysis, are given. Experimental work to determine the exact limits of solid solubility and its temperature dependence, and also the fields of solid solubility in both ternary systems, is currently in progress and will be reported later.

Two binary compounds, LaAlO₃ and 11Al₂O₃/La₂O₃ (La₂O₃ stabilized β -Al₂O₃), exist in the Al₂O₃-La₂O₃ system [14]. The binary compound LaFeO₃ exists in the La₂O₃-Fe₂O₃ system [15], while the AlFeO₃ compound in the Al₂O₃-Fe₂O₃ system is stable only at temperatures over 1300 °C, and decomposes into haematite solid solution and corundum solid solution at lower temperatures [16]. In the Mn₂O₃-Al₂O₃ system spinel solid solution forms above 1000 °C [17].

For experimental work, La(OH)₃ (Ventron, 99.9%), SrCO₃ (Ventron, 99.9%), MnO₂ (Ventron, 99.9%), Fe₂O₃ (Alfa, 99.9%) and Al₂O₃ (Alcoa, A-16, +99%) were used. The samples were mixed in ethyl alcohol, pressed into pellets and fired with intermediate grinding. During firing, pellets were placed on platinum foils. The compositions of the relevant samples are shown in Figs 3 and 4. The results were evaluated by X-ray powder analysis, scanning microscopy and EDS.

The ternary phase diagrams (subsolidus) are shown in Figs 3 and 4. The extent of solid solubility (at 1200 °C) is marked on the binary diagrams, but regions of solid solutions in the ternary diagrams are not shown. The phase diagram of the La₂O₃-Al₂O₃-Mn₂O₃ system is presented in Fig. 3. Tie lines exist between LaMnO₃-LaAlO₃ and LaAlO₃-Mn₂O₃. The solid solution can be described by the formulas LaMn_{1-x}Al_xO₃ (0 \leq x \leq 0.35) on the LaMnO₃ side, and LaMn_yAl_{1-y}O₃ (0 \leq y \leq 0.10) on the LaAlO₃ side.

The phase diagram of the La₂O₃-Al₂O₃-Fe₂O₃ system is presented in Fig. 4. The rate of formation of LaAl₁₁O₁₈ (β -Al₂O₃) from Al₂O₃ and La₂O₃ is extremely slow at temperatures below 1500 °C, and several months are needed for the synthesis [18].

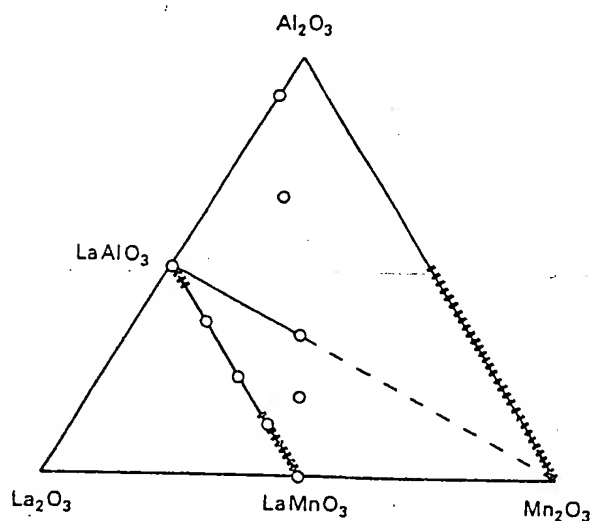


Figure 3 The phase diagram (subsolidus) of the La₂O₃-Al₂O₃-Mn₂O₃ system. Tie lines exist between LaMnO₃-LaAlO₃ and LaAlO₃-Mn₂O₃. The regions of solid solutions in the ternary

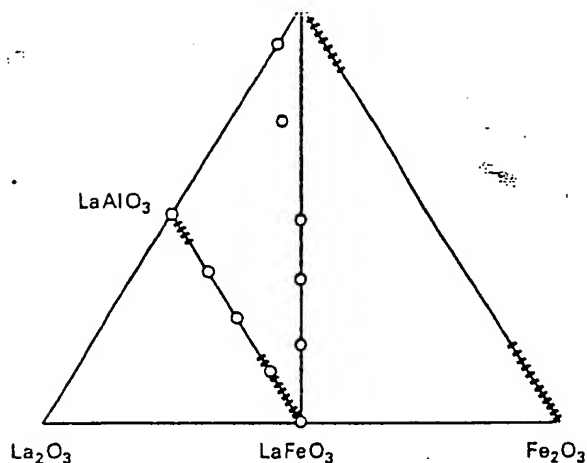


Figure 4 The phase diagram (subsolidus) of the La_2O_3 - Al_2O_3 - Fe_2O_3 system. Tie lines exist between LaFeO_3 - LaAlO_3 and LaFeO_3 - Al_2O_3 . The regions of solid solutions in the ternary diagram are not shown.

Therefore, it is not shown in the diagram. Tie lines exist between LaFeO_3 - LaAlO_3 and LaFeO_3 - Al_2O_3 . The solid solution can be described by the formulas $\text{LaFe}_{1-x}\text{Al}_x\text{O}_3$ ($0 \leq x \leq 0.40$) on the LaFeO_3 side and $\text{LaFe}_y\text{Al}_{1-y}\text{O}_3$ ($0 \leq y \leq 0.15$) on the LaAlO_3 side.

The results indicate that the degree of solid solubility is, at least to some extent, larger between LaAlO_3 - LaFeO_3 than between LaAlO_3 - LaMnO_3 .

Acknowledgements

This work was carried out as part of the "New SOFC Materials and Technology" project, ref. J0U2-CT92-0063. The authors would like to express their thanks to Dr Thomaž Kosmač for helpful discussions. The financial support of the Ministry of Science and Technology of Slovenia is gratefully acknowledged.

2. K. LEDJEFF, T. ROHRBACH and G. SCHAUMBERG, in Proceedings of the 2nd International Symposium on Solid Oxide Fuel Cells, edited by F. Grosz, P. Zegers, S. C. Singhal and O. Yamamoto, Athens (Commission of the European Communities, Brussels, 1991) p. 323.
3. N. Q. MINH, *Chemtech*, 2 (1991) 120.
4. K. KENDALL, *Ceram. Bull.*, 70 (1991) 1159.
5. F. GROSS, in Proceedings of the 2nd International Symposium on Solid Oxide Fuel Cells, edited by F. Grosz, P. Zegers, S. C. Singhal and O. Yamamoto, Athens (Commission of the European Communities, Brussels, 1991) p. 7.
6. H. TAGAWA, in Proceedings of the 3rd International Symposium on Solid Oxide Fuel Cells, edited by S. C. Singhal and H. Iwahara, Honolulu (The Electrochemical Society, Pennington, New Jersey, 1993) p. 6.
7. J. GLANZ, *Res. Dev.* 35(6) (1993) 36.
8. M. MOGENSEN and N. CHRISTIANSEN *Europhys. News* 24 (1993) 7.
9. N. Q. MINH, *J. Amer. Ceram. Soc.* 76 (1993) 563.
10. U. G. BOSSEL, in Proceedings of the 3rd International Symposium on Solid Oxide Fuel Cells, edited by S. C. Singhal and H. Iwahara, Honolulu (The Electrochemical Society, Pennington, New Jersey, 1993) p. 833.
11. J. MIZUSAKI, H. TAGAWA, T. SAITO, K. KAMITAMI, T. YAMAMURA, K. HIRANO, S. EHARA, T. TAKAGI, T. HIKITA, M. IPPOMATSU, S. NAKAGAWA and K. HASHIMOTO, *ibid.*, p. 533.
12. L. W. TAI, M. M. NASRALLAH and H. U. ANDERSON, *ibid.*, p. 241.
13. H. MATSUDA, T. ISHIHARA, Y. MIZUHARA and Y. TAKITA, *ibid.*, p. 129.
14. R. S. ROTH, J. R. DENNIS and H. F. McMURDIE (editors) "Phase diagrams for ceramists", Vol. VI 1987, supplement (The American Ceramic Society, Westerville, Ohio, 1987) Fig. 6438, p. 144.
15. *Idem*, "Phase diagrams for ceramists", Vol. I (The American Ceramic Society, Westerville, Ohio, 1964) Fig. 60, p. 53.
16. E. M. LEVIN, C. R. ROBBINS and H. F. McMURDIE (editors) "Phase diagrams for ceramists", Vol. II 1969, Supplement (The American Ceramic Society, Westerville, Ohio, 1969) Fig. 2095, p. 13.
17. *Idem*, *ibid.*, Fig. 2099, p. 15.
18. R. C. ROPP and G. G. LIBOWITZ, *J. Amer. Ceram. Soc.* 61 (1978) 473.

Received 18 May
and accepted 4 October 1994

BEST AVAILABLE COPY

THIS PAGE BLANK (USPTO)